Journal of Computational Neuroscience 17, 165–178, 2004

Annihilation of Single Cell Neural Oscillations by Feedforward and Feedback Control

FLAVIO FRÖHLICH* AND SAŠO JEZERNIK†
Automatic Control Laboratory, Swiss Federal Institute of Technology (ETH Zürich), Physikstr. 3, 8092 Zürich, Switzerland

Received March 16, 2004; Revised May 16, 2004; Accepted May 21, 2004

Action Editor: G. Bard Ermentrout

Abstract. Annihilation of neural oscillation by localized electrical stimulation has been shown to be a promising treatment modality in a number of neural diseases like Parkinson disease or epilepsy. The contributions presented in this manuscript comprise newly developed stimulation schemes to achieve annihilation of action potential generation and action potential propagation. The ability to achieve oscillation annihilation is demonstrated in computer simulations with a single compartment nerve cell model (annihilation of action potential generation), and with a multi-compartment nerve fiber model (annihilation of action potential propagation). Additionally, we show superiority of the new feedback based schemes over the feedforward schemes in terms of effectiveness, phase robustness, and reduced sensitivity to disturbances. At the end we propose a conditioned switched feedback control regime to be applied in actual applications, where oscillation annihilation is needed.

Keywords: Hodgkin-Huxley equations, oscillation annihilation, phase resetting analysis, electrical stimulation

1. Introduction

Annihilation of neural oscillation by localized electrical stimulation has been shown to be a promising treatment modality in a number of neural diseases like Parkinson disease or epilepsy. Kiss et al. (2002) showed suppression of rhythmic discharges in rat thalamic neurons by application of local high-frequency stimulation and related their findings to oscillation suppression in "tremor cells" in the sensorimotor thalamus of Parkinson patients. Benabid et al. (2000) found symptom alleviation (akinesia, rigidity, and tremor) in Parkinson patients by application of localized high-frequency stimulation in the subthalamic nucleus possibly resulting in oscillation desynchronization in sensory-motor loops responsible for the tremor. Tass (2003) suggested the separate, demand-controlled administration of high-frequency pulse trains to individual neuronal subpopulations to decrease firing synchrony as a possible stimulation protocol for patients with advanced Parkinson's disease. Gluckman et al. (2001) designed electric field feedback control to stop seizures in hippocampal slices. Controlling oscillatory behavior of single nerve cells and nerve cell populations by applying electrical stimuli is also expected to lead to methods to control epileptic seizures (Durand and Bikson, 2001). Guttman et al. (1980) achieved oscillation annihilation in experimental studies with the giant squid axon. Besides experimental demonstration of oscillation annihilation, several research groups have also demonstrated feedforward oscillation annihilation in simulations. For example, Cooley et al. (1965) observed oscillation annihilation by superimposing a brief depolarizing current pulse upon a constant bias current.

*Current address: Computational Neurobiology, University of California at San Diego, 9500 Gilman Drive, La Jolla, CA 92093-0357, USA.
†To whom all correspondence should be addressed.

Oscillation annihilation in Purkinje nerve fibers was explored in simulations by Chay and Lee (1984) and Guevara and Shrier (1987). These simulations led to explanation of oscillation annihilation (annihilation of action potential generation) due to coexistence of two stable states (bistability) of the nerve cell: a feedforward application of a short stimulus causes switching between the stable limit cycle and the stable fixed point. This phenomenon was also observed in various other biological systems Winfree (1987).

Many of these previous efforts in the field of oscillation annihilation have been focused on qualitatively changing firing patterns of neural populations. In this paper, new theoretical developments and simulation results towards conditioned and unconditioned feedback control of individual neurons involved in aberrant synchronous firing are presented. We thus focus on methods to achieve oscillation annihilation on a single nerve cell level. Specifically, we introduce new concept of feedback control and develop new control schemes to achieve oscillation annihilation at its origin (annihilation of action potential generation) and during oscillation transmission (annihilation of action potential propagation along the nerve membrane). The two types of feedback control schemes needed for annihilation of action potential generation and propagation are completely different, since they are based on different physical phenomena (and therefore different nerve models). The former application might be important in the research dealing with oscillation suppression of a population of nerve cells (like in epilepsy), and the latter in the research aiming for example at blocking of different central or reflex pathways.

Transmembrane stimulation of a nerve cell with a rectangular current pulse of sufficient amplitude and duration triggers an action potential, a transitory suprathreshold depolarization of the cell membrane. A constant current input of sufficient amplitude in turn generates a train of action potentials with constant amplitude and frequency that, after being generated at the location of the nerve stimulus delivery, propagate along the nerve cell membrane (e.g. along the axon to the end-effector organ).

The newly developed oscillation annihilation feedback schemes that interact with these phenomena were tested in computer simulations. So far, only simple feedforward schemes for annihilation of oscillation generation were known. Besides the design of new feedback control schemes, we also report on improvement of the already known feedforward control schemes. With different schemes, the external current is applied across the neuron body membrane in case of annihilation of action potential generation or across the axon in case of annihilation of action potential propagation.

The manuscript has the following structure: we first revisit feedforward annihilation of action potential generation (phase resetting) in a single compartment Hodgkin-Huxley model with stable limit cycle oscillation caused by a suprathreshold bias current. We determine a subspace of stimulus parameters (relative pulse onset t_c, pulse duration ΔT and amplitude I) where oscillation annihilation is achieved. This represents an augmentation of the analysis by Hahn and Durand (2001), who investigated oscillation annihilation with a single current pulse as a function of the onset of the pulse and its amplitude. Simulation results are then examined by performing the phase-plane and phase-resetting analysis. Next, we present our new idea, which is to use feedback control for oscillation annihilation, because oscillation annihilation by administration of a single pulse (feedforward) lacks robustness against variations in model parameters and stimulation timing. Feedback control in general has the advantage of exhibiting robustness in case of model uncertainty and external disturbances. The separately developed feedback control strategies for annihilation of neural oscillations are then tested in single compartment nerve model (annihilation of action potential generation) and in multi-compartment nerve fiber model (annihilation of action potential propagation). With annihilation of action potential propagation the situation is more complex than when annihilating the action potential generation (see below). The manuscript is concluded by a discussion section.

2. Methods

2.1. Nerve Models for Action Potential (AP) Generation and Propagation

The original Hodgkin-Huxley equations (1952) (listed in the Appendix) constituted the single compartment model used for examination of action potential generation, where the injected bias current was set to a constant value above rheobase ($I_{\text{inj}} = 8\ \mu\text{A/cm}^2$) causing a stable limit cycle oscillation with spiking frequency $f = 67.5$ Hz. For convenience the area of the membrane patch was set to 0.1 mm^2 so that the used bias current of 8 μA/cm^2 equaled 8 nA.

The multicompartment nerve fiber model used for simulation of action potential propagation consisted of 10 identical compartments and was a discrete nerve fiber model of a myelinated axon as in McNeal (1976).

The ionic membrane currents flowed only at the nodes of Ranvier. The saltatory propagation mechanism of an action potential along a myelinated axon justifying such a discrete multicompartment model was first shown experimentally by Huxley and Stämpfli (1948) and in computer simulations by Fitzhugh (1962). The total inflowing current I_j into node (compartment) j from the two neighboring compartments $j-1$ and $j+1$ equals:

$$I_j = \left(\frac{G_i}{1 + \frac{G_i}{G_o}} \right) (V_{j-1} - 2V_j + V_{j+1}) \qquad (1)$$

where G_0 denotes the extracellular conductance per unit area, and V_j the membrane voltage of compartment j. The membrane voltage at compartment j is thus determined by

$$C_m \frac{dV_j}{dt} = I_j - I_{\text{ionic},j}. \qquad (2)$$

The internodal, axoplasmatic conductance per unit area G_i is given by:

$$G_i = \frac{d}{4\rho_i L l} \qquad (3)$$

where d is the axon diameter, ρ the axoplasm resistivity, L the internodal length, and l the nodal gap width (McNeal, 1976). The used numerical values are listed in Table 1. For $D = 20\ \mu$m, G_i equals 63.6 mS/cm^2.

Following the literature (Rattay, 1990; Weiss, 1996), we assume that $G_o \gg G_i$. Thus, the eq. (1) reduces to:

$$I_j = G_i(V_{j-1} - 2V_j + V_{j+1}) \qquad (4)$$

Table 1. Variables determining intranodal, axoplasmatic conductance G_i used in the multi-compartment nerve fiber model. Adapted from McNeal (1976).

Variable	Value
Ratio of axon to fibre diameter d/D	0.7 (Goldman and Albus, 1968)
Axoplasmatic resistivity ρ_i	110 Ω cm (Stämpfli, 1952)
Ratio of internodal length to fiber diameter L/D	100 (Hursh, 1939)
Nodal gap width l	2.5 μm (Dodge and Frankenhaeuser, 1959)

In the multicompartment model, oscillation was generated by injecting a constant bias current above rheobase ($I_{\text{bias}} = 8$ nA) into the first compartment. The action potentials then propagated along the other nine compartments.

2.2. *Feedforward Oscillation Annihilation in Single Compartment Model (Annihilation of AP Generation)*

We started our research by systematically studying the effect of a single rectangular stimulation pulse on oscillatory behavior generated by a sustained constant bias current in a single compartment model. This research phase represents an augmentation of earlier work by Hahn and Durand (2001), where two rectangular pulse parameters (onset of pulse t_c and its amplitude I) were systematically varied to achieve oscillation annihilation. In our case, the stimulation pulse was described by three basic feedforward pulse parameters: onset of the pulse t_c, pulse duration ΔT, and pulse amplitude I. It is clear that ΔT represents an additional degree of freedom that was neglected in Hahn and Durand (2001). The onset of the pulse t_c was defined as the time interval between the maximum value of the action potential preceding the stimulus and the actual onset of the pulse. The subspace of the pulse parameters used for simulation was a regularly sampled cuboid. Table 2 lists the examined intervals and used increments for all three parameters. For each combination of these values, the time-course of the membrane voltage in the single compartment model was determined by simulations (Matlab SIMULINK, ode 5 Dormand-Prince solver, simulation time step $T_s = 0.01$ ms). For each time-course, a phase-resetting analysis was performed by first determining the time θ_{new} elapsed between the peaks of the action potentials preceding and following the rectangular stimulus. Thereof, the relative temporal phase shift θ_r of the disturbed oscillation, defined as

$$\theta_r = \frac{\theta_{\text{new}} - \theta_{\text{old}}}{\theta_{\text{old}}}, \qquad (5)$$

Table 2. Parameters for feedforward application of a single current pulse in single compartment nerve model.

Variable	Increment	Examined interval
Pulse onset t_c	0.5 ms	[5, 15] ms
Pulse duration ΔT	0.1 ms	[0.1, 2.0] ms
Pulse height I	1 nA	[1, 20] nA

was determined, where θ_{old} denotes the oscillation period in the undisturbed case. Based on θ_r, three cases can be distinguished. If $\theta_r < 0$, an advance of the following action potential occurred. If $\theta_r > 0$, then the consecutive action potential was delayed compared to the undisturbed oscillation. In case of oscillation annihilation, θ_{new} and thus θ_r are infinite (phase singularity).

For each value of the pulse onset t_c, a 2-dimensional phase-resetting map was computed. In the phase-resetting map at a fixed time t_c, the abscissa denotes the pulse duration ΔT, while the pulse amplitude I is marked on the ordinate. The value of θ_r corresponding to each simulation was represented by a square with a certain gray-scale level. Dark gray tones display a relative phase shift smaller than zero, whereas relative phase shifts greater than zero are shown in light gray tones. White squares show the regions of phase singularities where the oscillation was suppressed (annihilation regions).

In the additional phase-plane analysis we have examined the resulting system trajectories in two-dimensional phase subspace (the full system dimension is four). From plotting separate phase-plane projections for the pairs (m, V), (h, V), and (n, V) with m, h, and n being sodium activation and inactivation and potassium activation respectively, it became clear that projection of the system trajectory into the V-n-plane was sufficient for understanding of oscillation annihilation (and AP generation).

Since the geometric phase shift is the relevant parameter in the phase-plane analysis, conversion from temporal $\phi = \frac{\tau}{T}$ to geometric phase σ was required. Geometric phase σ along a limit cycle arising from a dynamic system governed by N differential equations of the form $\frac{du_k}{dt} = f_k(u)$ is defined as a relative portion of the length L of the limit cycle and is a function of the elapsed time τ (Oprisan and Canavier, 2002):

$$\sigma = \frac{1}{L} \int_0^{\tau} \left(\sqrt{\sum_{k=1}^{N} (f_k(u))^2} \right) dt. \tag{6}$$

2.3. *Feedback Oscillation Annihilation in Single Compartment Model (Annihilation of AP Generation)*

Based on the phase-plane analysis of feedforward annihilation of neuronal oscillation we were then able to formulate the corresponding feedback control problem.

Two different feedback control strategies for suppressing stable oscillations in the Hodgkin-Huxley single compartment neuronal model were developed and subsequently tested in computer simulations. The first scheme is straight-forward: a reference voltage $V_{\text{ref}} = 0$ mV for the output V is specified. The controller forces V to reach zero and to stay there (*permanent control*). In the second scheme, the controller is first used to move the state of the system into the region of attraction of the stable fixed point ($V_{\text{ref}} = 5$ mV), which exists due to the injected bias current I_{bias}. After reaching the region of attraction (sufficient time is needed to do so), the controller is switched off (*interval control*). The time interval during which the controller is active is denoted by ψ and called *control interval*.

For permanent feedback control of the membrane voltage a state feedback linearization controller was designed. The differential equation describing the membrane voltage V in the Hodgkin-Huxley model was transformed into an equivalent linear system by applying a transformation called state feedback linearization. This transformed our nonlinear dynamical system description into an equivalent description consisting of linear differential equations (Khalil, 2002). Following this transformation, a linear state controller was designed for the transformed system. The resulting final state feedback controller yields a current I_{inj} which forces the membrane voltage V to asymptotically track a given reference voltage V_{ref}. The control law of the state feedback controller equals:

$$\begin{aligned} I_{\text{inj}} = & -\bar{G}_K n^4 (E_K - V) \\ & - \bar{G}_{\text{Na}} m^3 h (E_{\text{Na}} - V) \\ & - G_m (V_{\text{rest}} - V) \\ & + C_m (\dot{V}_{\text{ref}} + K(V_{\text{ref}} - V)) \end{aligned} \tag{7}$$

The dynamics of the tracking error $e = V_{\text{ref}} - V$ is described by a first-order differential equation with time constant $\tau = 1/K$:

$$\dot{e} + Ke = \frac{I_{\text{bias}}}{C_m} \tag{8}$$

where K represents the feedback gain of the controller, and I_{bias} denotes the sustained bias current. Preliminary simulations suggested $K = 10\ \text{ms}^{-1}$ as a reasonable value (yielding $\tau = 0.1$ ms). For ease of presentation, K was normalized by division by $1\ \text{ms}^{-1}$ in the following. The state feedback controller was also compared with a simple proportional controller (which had the

same feedback gain) in order to show superior performance of the former.

The difference between the two schemes in terms of the reference voltage is that the permanent controller enforces zero membrane voltage all the time. Other inflowing currents represent disturbances that are continuously counteracted by the controller. In the second scheme, the system with the injected bias current is transientlly moved to the second equilibrium (stable fixed point inside the limit cycle) and remains there. No controller action is required afterwards (energy minimization).

The performance of the permanent feedback controller and its ability to annihilate action potential generation were systematically examined in simulations for different controller gains, model-controller mismatch, and additional superimposed membrane voltage disturbances. The effect of the feedback gain K on the maximum current amplitude and the tracking error was tested as well. Systematical testing of the second (switched) feedback control strategy included testing the annihilation condition in terms of the necessary minimum control interval (time during which the controller is switched on), and the relative switching time onset. Phase-plane analysis as used in the feedforward annihilation of AP generation was performed as well.

2.4. *Feedback Oscillation Annihilation in Multi-Compartment Model (Annihilation of AP Propagation)*

The feedback control problem of annihilation of AP propagation is different from annihilation of AP generation. When APs propagate along the nerve fiber, the corresponding physical model corresponds to coupled single compartment models, where currents flow between the adjacent compartments. Due to nonstationary nature of these neighboring currents the system properties like equilibria and stability continuously change as the injected current is a bifurcation parameter (Fukai et al., 2000). Thus it is clear that in order to achieve annihilation of AP propagation with a localized feedback controller (whose current is injected into a single compartment in the multicompartment model), only the permanent control scheme will work. However, in order to achieve additional energy saving, the permanent feedback controller with zero reference voltage can be used in a switched regime, based upon detection of an initiation of an AP (for example, detection of a sufficient, suprathreshold depolarization). The controller should be switched on until the membrane voltage falls below the threshold. This will enable annihilation of AP propagation along other compartments with a lesser amount of energy. Such a switched regime is typically denoted by conditioned (vs. unconditioned) nerve stimulation. The stimulation is conditioned upon the detection of an initiated AP.

The above schemes for annihilation of AP propagation were tested in simulations with the multicompartment nerve fiber model. During these simulations, the controller was set to control the membrane voltage of the fifth compartment. The constant bias current needed for the generation of the APs was injected into the first compartment. The switched control scheme was evaluated for different values of the control interval ψ.

3. Results

In the first two parts of this section, we report on oscillation annihilation of AP generation in single compartment models, the last part is dedicated to the oscillation annihilation of AP propagation in multicompartment nerve fiber model.

3.1. *Feedforward Oscillation Annihilation in Single Compartment Model*

The results of application of a feedforward current pulse in the single compartment model are shown in Fig. 1. Phase delay ($\theta_r > 0$, second panel in Fig. 1), phase advance ($\theta_r < 0$, bottom panel in Fig. 1) and oscillation annihilation (third panel in Fig. 1) were achieved as a specific amount of charge was injected into the membrane at the right moment. For comparison, the top panel shows the time course of the membrane voltage in absence of any perturbation.

The phase-resetting maps for feedforward current pulses described by three parameters (3 degrees of freedoms) are shown in Fig. 2. In all maps, there exist either two or three separate regions: a region with $\theta_r > 0$ (phase delay, shown in light grey tones), a region with $\theta_r < 0$ (phase advance, shown in dark grey tones), and an annihilation region (θ_r infinite, white region). These maps were calculated for $t_c \in [2.5, 12.5]$ ms. By increasing t_c, the smoothness of the transition between these regions increased. In all phase resetting maps, the annihilation region arose at the border between the phase delay and the phase advance region. For $t_c < 7.5$ ms and $t_c > 9.5$ ms, no annihilation

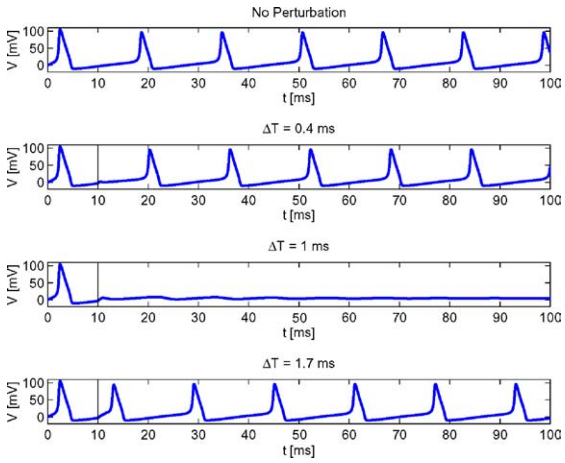

Figure 1. Feedforward oscillation annihilation. Top panel: Neuronal oscillation without perturbation. Remaining panels: Oscillation perturbed by a current pulse (pulse onset $t_c = 7.54$ ms, amplitude: 14 nA, duration: ΔT). Vertical line indicates the onset of the feedforward pulse. Third panel shows annihilation of oscillation (action potential generation).

regions were found. Those values of t_c determine the boundaries of the vulnerable interval, an interval during which oscillation annihilation by application of a single current pulse can be achieved. Our results show that additionally to pulse onset t_c and pulse amplitude I, pulse duration ΔT is an important parameter in the feedforward oscillation annihilation scheme. This parameter adds one degree of freedom. As it can be seen from Fig. 2, varying ΔT for a given pair (t_c, I) determined whether advance, delay or oscillation annihilation occurred.

Figure 3 shows the three different cases from Fig. 1 in phase plane: phase delay (A) for $\Delta T = 0.5$ ms, annihilation (B) for $\Delta T = 1.2$ ms, and phase advance (C) for $\Delta T = 2.0$ ms.

In all three cases, the trajectory initially moved away from the limit cycle. In case A, it was again attracted by the limit cycle after termination of the pulse. No annihilation took place. The trajectory was forced to take a detour before coinciding again with the limit cycle

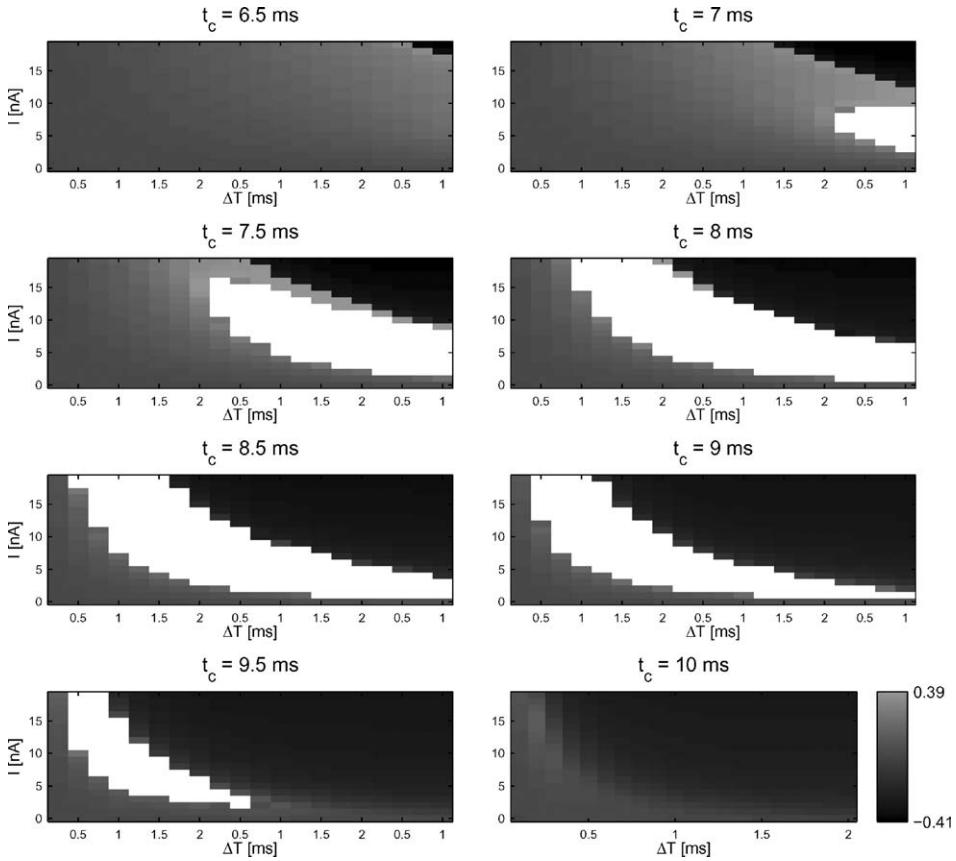

Figure 2. Phase-resetting maps for different values of pulse onset t_c. Dark gray tones display a relative phase shift $\theta_r < 0$ (phase advance). Light gray tones represent a relative phase shift $\theta_r > 0$ (phase delay). White areas show the regions of phase singularities where the oscillation was suppressed (annihilation regions).

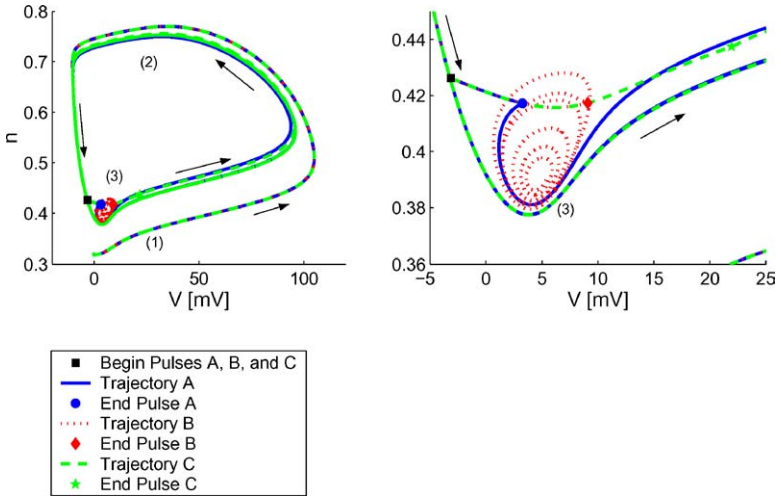

Figure 3. Left: Phase-plane plot of potassium activation n and membrane voltage V. Single current pulse stimulation (t_c = 10 ms, $I = 14$ nA) for durations $\Delta T = 0.5$ ms (A), $\Delta T = 1.2$ ms (B), and $\Delta T = 2.0$ ms (C) were delivered at location marked by a full square. The arrows depict the temporal evolution. While in cases A and C the trajectories got just temporarily disturbed and have afterwards returned to the stable limit cycle, in case B the trajectory converged to the stable fixed point. Label (1): Resting fixed point for $I_{\text{inj}} = 0$ nA. Label (2): Stable limit cycle for $I_{\text{inj}} = 8$ nA. Label (3): Stable fixed point for $I_{\text{inj}} = 8$ nA. Right: Expansion of region of interest in left plot. In case A, the trajectory was forced to make a detour around the region of attraction of the stable fixed point causing a phase delay, in case C the trajectory took a shortcut resulting in a phase advance. In case B, the trajectory moved into the region of attraction of the stable fixed point.

(phase delay). In case B, the trajectory was attracted by the stable fixed point, which was approached in a spiral-shaped curve. The current stimulus displaced the state in such a way that it lay close enough to the stable fixed point in order to spiral in (region of attraction (ROA)). On the contrary, in case C, the trajectory took a shortcut back to the stable limit cycle, without being largely affected in its course (phase advance).

With these simulations we have shown that with an appropriate choice of the stimulus parameters, bistability can be exploited to switch between oscillatory and resting state of the neuron (when firing in an oscillatory way due to an injected bias current). Figure 4 depicts the qualitative structure of the relevant excerpt of the phase plane. The resulting type of dynamics is determined by the state of the system after application of the stimulation pulse. The stable fixed point lies inside the limit cycle, and this explains why choosing initial conditions lying outside the limit cycle will necessarily lead to a stable oscillation in absence of any perturbation. The limit cycle and the fixed stable point lie close together; thus, small changes in pulse duration and amplitude can substantially change the system's behavior. Figure 3 also illustrates that a short current pulse mainly changes V and keeps potassium activation n almost constant.

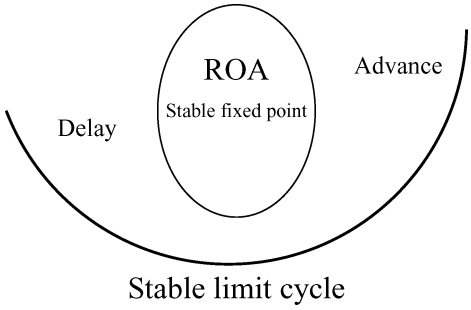

Figure 4. Qualitative structure of the projected phase-plane. The region of attraction of the stable fixed point is denoted by ROA. The resulting type of behavior is determined by $x_{(t_c+\Delta T)} = (V, m, h, n)'_{(t_c+\Delta T)}$. If the trajectory does not reach the ROA of the stable fixed point upon the termination of the perturbation pulse, a phase delay occurs. If the trajectory crosses the ROA, a phase advance can be observed. Oscillation annihilation occurs when the trajectory at the end of the stimulation pulse ($t = t_c + \Delta T$) reaches the ROA.

The coexistence of a stable limit cycle and a stable fixed point is in agreement with (Fukai et al., 2000), who carried out comprehensive bifurcation analysis for the Hodgkin-Huxley model. Increase of the sustained bias current causing the oscillation leads to a shrinkage of the region of attraction of the stable fixed point, which at some point eventually becomes unstable. This

happens for $I > 9.78$ nA (which was confirmed by the use of the numerical bifurcation analysis software *locbif* (Khibnik et al., 1992). Thus, for the used model the range of bistability is limited with standard parameters. However, other regions of bistability exist with different values of other bifurcation parameters as potassium/sodium maximum conductances etc. (see for example (Fukai et al., 2000) and its companion paper, first and second parts for more information). Also, the realistic models and actual nerve cells are more complex and will contain other cases of bistable bifurcation diagram regions (since bistability of nerve cells was also demonstrated in experiments). So, since bistability was experimentally demonstrated, our proposed control techniques can be used in order to achieve oscillation annihilation based on the bistability mechanism.

The shifts in geometrical phase (determined from phase plane analysis) are directly related to the temporal phase shift. The relation between the geometrical phase σ and the temporal phase $\phi = \frac{\tau}{T}$ for the Hodgkin-Huxley equations with a constant bias current $I_{\text{bias}} = 8$ nA and an oscillation frequency $f = 60.2$ Hz is shown in Fig. 5. It follows that within the vulnerable interval $\phi \in [0.57, 0.69]$, a linear relationship between geometrical and temporal phase can be assumed. Thus, a shift in geometrical phase resulting from the application of a short stimulus is proportional to the corresponding temporal phase shift.

In summary, with the feedforward current pulse scheme, oscillation annihilation in single compartment model can be achieved. However, there exist several limitations of the feedforward scheme. The most critical limitations are explicit phase dependency and high sensitivity to model parameters and disturbances, as inherent in feedforward schemes. These limitations are overcome by newly developed feedback control schemes.

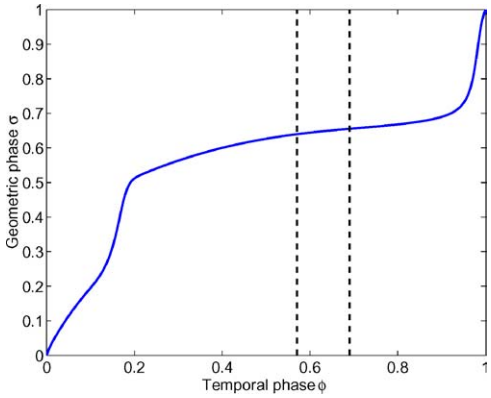

Figure 5. Geometric phase σ as a function of temporal phase ϕ determined by simulation (Hodgkin-Huxley equations with bias current $I_{\text{bias}} = 8$ nA). The vertical dashed lines delimit the vulnerable interval, where oscillation annihilation was achieved.

3.2. *Feedback Oscillation Annihilation in Single Compartment Model*

3.2.1. Permanent Control. The permanent control scheme is a straight-forward approach to oscillation annihilation, since the feedback controller enforces zero membrane voltage by counteracting currents that would lead to de- or hyperpolarization. The effect of varying the feedback gain K on the controller performance was explored first. Repeated simulations with different K values revealed that the interval $K \in [1, 10]$ constitutes a reasonable choice for good oscillation annihilation. Smaller values of K caused high steady-state errors, whereas values of $K > 10$ caused very high peaks in controller output I_{inj} (stimulation current). The choice of the feedback gain K is thus subject to a trade-off between steady-state error, tracking error dynamics, and maximum injected current amplitude. The steady-state error arises from the constant bias current I_{bias} causing the oscillation. It could be eliminated by adding an integrator to the control scheme. The peak value of I_{inj} is a function of the time instant when the controller is switched on (relative to an earlier AP) and of the feedback gain K. High peak values occurred for large values of K and for a switch-on (activation) time T_a close to the moment where the membrane voltage reached its maximum value. The obtained relationship is shown in Fig. 6. This figure shows the maximum absolute value of the controller output as a function of K and activation time T_a. The permanent controller should thus be switched on in an instant when the membrane voltage is close to the resting voltage to avoid high injected current amplitudes.

In this place we also want to show results stemming from comparison of the performance of the state feedback controller versus a proportional controller as used in voltage clamp experiments. The fundamental difference between the feedback linearization controller and a proportional controller is that the former takes into account the inherently nonlinear dynamics of the voltage-gated ion channels, and that the proportional controller design ignores the nonlinear membrane kinetics, which leads to a worse tracking performance. This is shown in Fig. 7. A significant difference in tracking performance can be observed.

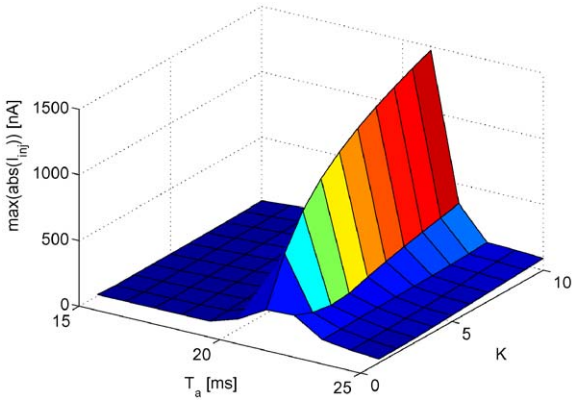

Figure 6. Permanent control scheme: the maximum absolute value of the controller output I_{inj} as a function of the feedback gain K and the activation time T_a (representing the moment when the controller was switched on). High peak values occurred for activation time T_a close to 22.4 ms where the membrane voltage V reached its maximum value.

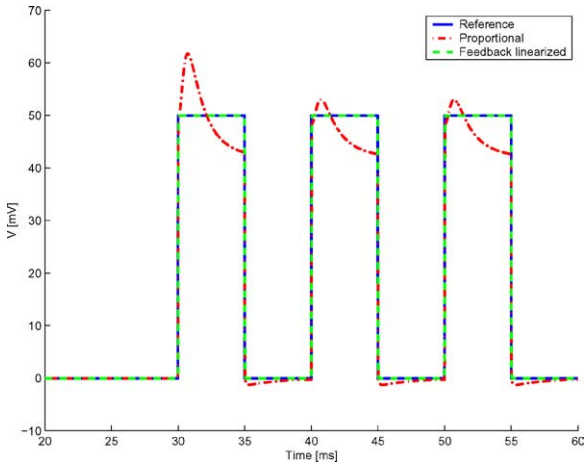

Figure 7. Tracking of a rectangular reference voltage time course (solid line). The trace labelled *proportional* shows the membrane voltage for the proportional controller. The trace labelled *feedback linearized* represents the membrane voltage for the new feedback linearization controller. Tracking performance is clearly better for the latter control scheme.

The ability of the state feedback controller to reject disturbances was tested by administering a brief, rectangular perturbation to the membrane voltage at $t = 70$ ms (height: 40 mV; duration: 10 ms). Besides a short transient response, the time-course of V was not disturbed (Fig. 8), and complete oscillation annihilation could be achieved. Furthermore, the steady-state controller current level at the end of this recording was such that it just cancelled the bias current, meaning that the net transmembrane current equaled zero.

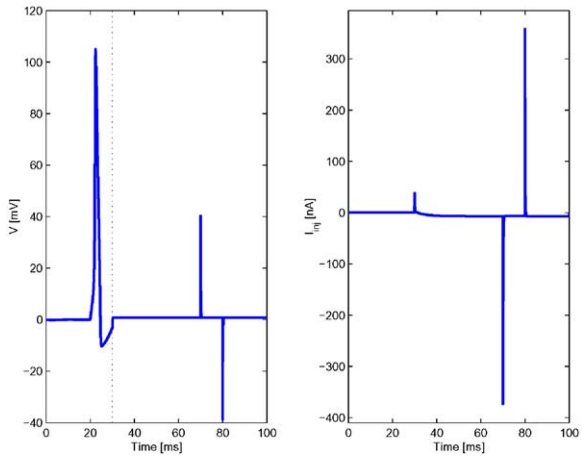

Figure 8. State feedback control: permanent control scheme. Annihilating oscillation caused by a constant, depolarizing bias current ($I_{\text{bias}} = 8$ nA). Membrane voltage V (left) and controller output I_{inj} (right). $K = 10$. Vertical dashed line: controller was switched on. Rectangular perturbation of V (height: 40 mV; duration: 10 ms) administered at $t = 70$ ms, did not lead to a generation of an action potential.

3.2.2. Interval Control. As already mentioned above, the interval control scheme works by moving the system trajectory close to the stable fixed point located at 5 mV (membrane voltage), such that after the controller is switched off, the system trajectory converges and remains in this system equilibrium. In the interval control scheme, the duration of the control interval ψ (during which the state feedback controller was switched on) was the most important control parameter. For small values of ψ, the state of the system did not reach the region of attraction of the stable fixed point (top panels in Fig. 9: $\psi = 0.5$ ms); no oscillation annihilation occurred. By extending the control period ψ to 2.0 ms, the region of attraction of the stable fixed point was reached and annihilation took place (bottom panels in Fig. 9). This means that $\psi \geq 2.0$ ms guaranteed oscillation annihilation in the interval control scheme. The minimum control interval depends on the model parameters and model-controller mismatch. To guarantee reaching the region of attraction of the stable fixed point, it is better to use a larger control interval.

Phase-space analysis of the system behaviour during interval control is shown in Fig. 10. Trajectory D ($\psi = 0.5$ ms) converged back to the stable limit cycle after the end of control interval ψ. Trajectories E ($\psi = 2$ ms) and F ($\psi = 10$ ms) were attracted by the stable fixed point. This illustrates that oscillation

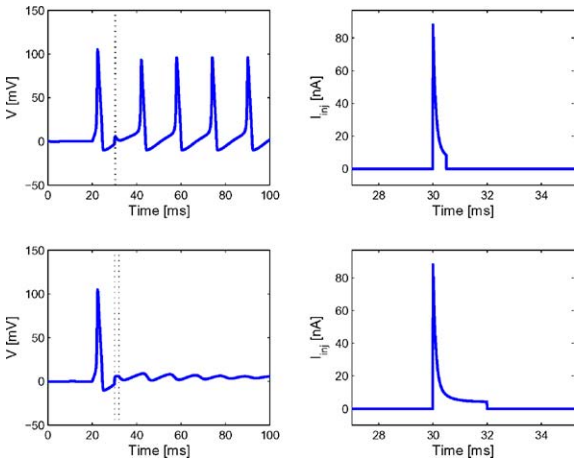

Figure 9. State feedback control: interval control scheme to annihilate oscillation caused by a constant, depolarizing bias current ($I_{\text{bias}} = 8$ nA) by switching on the feedback controller ($K = 10$) for duration ψ (marked by dashed lines). Membrane voltage V (left) and controller output I_{inj} (right). Top panels: controller switched on at $t = 30$ ms for a duration of $\psi = 0.5$ ms. Bottom panels: controller switched on for $t \in [30, 32]$ ms. Note the different time scales used in the two columns.

annihilation can be achieved regardless of the relative onset of the control signal (switch-on time) by choosing a large enough control interval ψ (robustness of the interval scheme to membrane voltage phase). Furthermore, a comparison of the latter two phase-space trajectories shows that an increase of ψ diminishes the amplitude of the transient process before reaching the stable fixed point.

The interval feedback control scheme thus achieves oscillation annihilation in the same way as the feedforward scheme, but with following advantages: robustness to switch-on (delivery) time (parameter t_c in the feedforward scheme) and robustness against other disturbances (as also demonstrated in results concerning the permanent feedback scheme). In the presence of disturbances that will after oscillation annihilation move the system state away from the region of attraction of the stable fixed point, the interval controller will need to be switched on again. Thus, the switch-on time can be conditioned upon deviation of the membrane voltage V from the V_{fixed} point. This will lead to a conditioned stimulation interval control scheme to achieve annihilation of action potential generation.

3.3. *Feedback Oscillation Annihilation in Multicompartment Model (Annihilation of AP Propagation)*

Oscillation annihilation with single pulse stimulation could not be achieved with the multicompartment model except when the feedback stimulation pulse was applied to the first compartment representing the axon hillock (location of the AP generation—analog to oscillation annihilation of AP generation in single compartment models). In other cases the inflowing currents

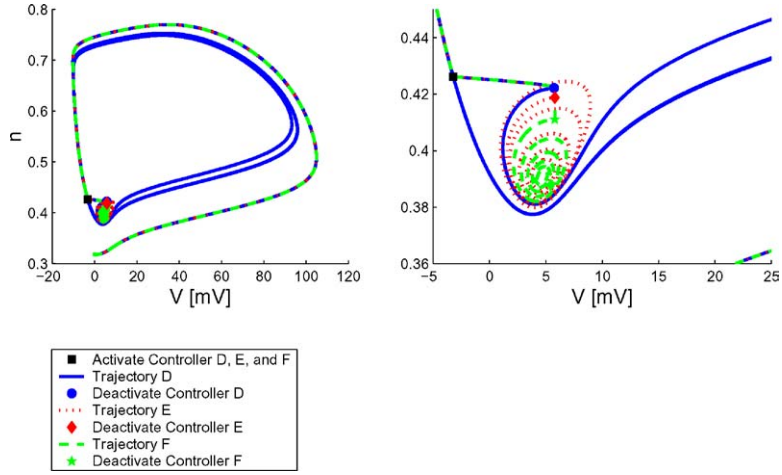

Figure 10. State feedback control: interval control. Left: Phase-plane plot of potassium activation n and membrane voltage V. State feedback controller was switched on at $t = 30$ ms for $\psi = 0.5$ ms (D), $\psi = 2.0$ ms (E), and $\psi = 10.0$ ms (F). Controller parameter $K = 10$. Trajectory D returned to the limit cycle, whereas trajectories E and F spiraled into the stable fixed point. Right: Expansion of the region of interest. The convergence of trajectory F to the stable fixed point was faster than the convergence of trajectory E.

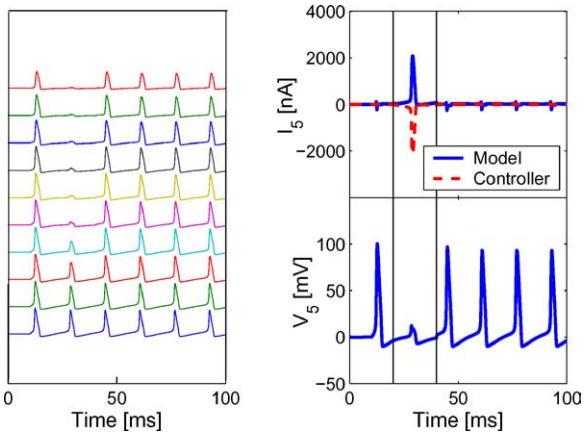

Figure 11. Left: Membrane voltage V of compartments 1 to 10. Compartment 1 was stimulated with a constant bias current $I = 8$ nA (onset at $t = 10$ ms). APs propagated from compartment 1 to 10. The state feedback controller for compartment 5 was active for $t \in [20, 40]$ ms and has annihilated propagation of the second AP. Top right: Current I_5 flowing into compartment 5 (solid line). Current injected by controller (dashed line). Bottom right: Membrane voltage V_5 of compartment 5. The vertical solid lines confine the control interval, during which the feedback controller was switched on.

from the neighboring compartments hindered the system from staying in the region of attraction of the transientlly existing stable fixed point. The possibly arising stable and unstable equilibria thus cannot be used as a set-points of the interval controller due to their transient nature. On the other hand, the permanent state feedback controller enabled oscillation annihilation in the multicompartment model independent of the location of control action (compartment where the annihilating stimulation was applied). However, inactivating the controller as in the interval control scheme used in the single compartment model led to an immediate restart of the oscillation (Fig. 11). The top right panel in Fig. 11 shows the current stemming from the neighboring compartments flowing into the stimulated compartment (solid line) and the externally injected current that was applied by the feedback controller (dashed line). The bottom right panel shows the time course of the membrane voltage at the corresponding axonal node. The controller was switched on for $t \in [20, 40]$ ms. Complete annihilation robust to electrode positioning can thus only be achieved by permanent control or conditional triggering of the permanent controller (which requires on-line action potential detection). The conditioning can be done on measured deviation from the resting membrane voltage.

4. Discussion

4.1. *Conditions for Oscillation Annihilation in Single Compartment Model (Annihilation of AP Generation)*

As we have seen, there exists an interval $[V_{\min}, V_{\max}]$ for V where the trajectory in the projected phase-plane is close enough to the stable fixed point to switch from the stable limit cycle to the stable fixed state (Figs. 3 and 4). Since the fixed point state is close to the resting equilibrium state, the ionic currents flowing when the state is in this region are small. By neglecting them, an approximate condition on the injected charge Q_{inj} for feedforward oscillation annihilation can be formulated:

$$V_{\min} < V_i + \frac{Q_{\text{inj}}}{C_m} + \frac{Q_{\text{bias}}}{C_m} < V_{\max} \tag{9}$$

where C_m is the membrane capacitance and V_i the membrane voltage at the onset of the pulse. The boundary values $V_{\min}$ and $V_{\max}$ can then be easily transformed into boundary values $Q_{\min}$ and $Q_{\max}$ for the injected charge Q_{inj}. From Fig. 2 we see that almost all annihilation regions have in fact a shape, which can be described as an area bounded by two hyperbolic curves. Since the charge is proportional to the following product: $Q_{\text{inj}} \alpha\, I \Delta T$, the approximate condition for annihilation equals:

$$\frac{Q_{\min}}{\Delta T} < I < \frac{Q_{\max}}{\Delta T} \tag{10}$$

.

This approximation is valid for application of the pulse for system states with V close to zero and lying close to the fixed point ($n \approx 0.4$) (horizontal displacement of the system state due to a feedforward current pulse). Thus, for a feedforward pulse it is advantageous to apply it with the onset of pulse t_c such that the application will occur when $V \approx 0, n \approx 0.4$. The feedback interval control will in turn be able to easily drive the system from any point of the limit cycle towards the stable fixed point (phase robustness). Jahangiri et al. (1997) developed an algorithm to predict the occurrence of oscillation annihilation in a Hodgkin-Huxley model with increased extracellular potassium concentration. Their main concept was to estimate the charge needed to move the membrane voltage V to the stable fixed point V_s under the assumption that the rate of change of the membrane voltage is constant within a short time interval in case of no external perturbation.

This allowed the derivation of a similar equation relating pulse duration ΔT to amplitude I with an additional $\frac{dV}{dt}$ term that includes the effects of the bias and ionic currents:

$$I = \frac{1}{\Delta T}\left((V_s - V) - 0.5\left(\frac{dV}{dt}\right)_i \Delta T\right) \qquad (11)$$

where $(\frac{dV}{dt})_i$ is the slope of the membrane voltage time-course at the onset of the current stimulus. However, this procedure does not take into account the fact that moving the system into the region of attraction of the fixed stable point without reaching V_s is already sufficient to achieve oscillation annihilation with a single current pulse. Thus, the latter can be achieved by a much richer set of parameter triples $(I, \Delta T, t_c)$ than predicted by Jahangiri et al. (1997) (as shown in this manuscript).

4.2. Comparative Assessment of Control Schemes

In this manuscript we have developed (and tested in simulations) different control schemes for annihilation of neural oscillation. For annihilation of AP generation, the control schemes work by moving the state of the system from one stable state (limit cycle) into the region of attraction of another stable state (stable fixed point). This control principle clearly outperforms brute force hyperpolarization, which can cause disturbing adaptation and polarization/damage of the involved neural tissue weakening stimulation efficiency. However, the principles of feedforward pulse stimulation and state feedback control differ. Single current pulse stimulation is a feedforward control strategy, which achieves oscillation annihilation only in a limited vulnerable interval for certain parameter values describing the stimulation pulse. A further disadvantage of the feedforward control scheme is the lack of robustness. In case of mismatch between the model and the nerve cell to control, the aforehand determined single pulse stimulation parameter triplet $(I, \Delta T, t_c)$ might not achieve oscillation annihilation anymore. By using a feedback interval control scheme to drive the trajectory towards V_s, one actually also avoids the problem of sensitivity and necessity of exact calculation of the required feedforward pulse parameters that would also be difficult because of the necessity of exact parameter identification. The feedback control schemes should thus be preferred for oscillation annihilation.

For annihilation of AP propagation along the axon, a feedback controller that is permanently switched on is actually required (single current pulse feedforward schemes will not work). Another possibility to achieve blocking with potentially less energy is via a conditioned switching of the permanent feedback controller. Again, the conditioned feedback control schemes should be preferred over conditioned feedforward schemes because of reduced sensitivity.

Here we would also like to mention that we have recently also designed a feedback controller to control the AP generation by controlling the ion channel opening/closing. This work was published in Fröhlich and Jezernik (2003).

The model we have used in the simulations contains only the potassium, sodium, and leakage current terms (standard H-H model). However, many more complex models exist in the literature so that these models can be taken as a starting point instead. It is easy to include in the model also other currents such as calcium currents and even different modulating agents. The control design can with more or less effort be extended to these more complex models. However, even control designs based on simplified models are known to typically show good performance when applied to real systems due to their feedback action.

By deploying one of the investigated approaches to control real biological systems, moreover a trade-off between ease of implementation and required performance must be sought. The feedforward approach requires a simple device producing current pulses. In general, the course of the membrane voltage does not have to be measured or estimated. On the other hand, to determine correct feedforward pulse parameters, the relative AP phase and thus the membrane voltage needs to be known. For example, to determine correct pulse parameters, Jahangiri et al. (1997) had to estimate the terms V and $\frac{dV}{dt}$. Also, in case of disturbances, the lack of feedback can lead to a decrease in efficiency in annihilation of oscillations. It can easily happen that the feedforward schemes (will) fail in practice. It is thus better to use feedback schemes instead, even though with these the state variables must be measured or estimated. Still, powerful existing current technologies should enable practical realization in terms of sampling time, memory, and computational power requirements. The more difficult development will be providing electrode stability for electrodes needed for neurographic recording and direct current stimulation. Interesting and challenging remaining development will be the

development towards presented feedback schemes where transmembrane stimulation and recording will be substituted by extracellular stimulation and recording. Of course, some modifications will need to be made then, as the extracellular stimulation will lead to not only one, but several (concurrent) nodal currents. The focus of the current simulations was on the patch-clamp recording/stimulation techniques, as in the first research phase we have addressed oscillation annihilation in single nerve cells only. So the first experimental verification step should apply the patch-clamp techniques as well. On the other hand, considering any more complex system given by multiple nerve cells will clearly need further research to modify the developed methods.

A disadvantage of the feedback schemes might be that the current amplitudes of the state feedback controller might be higher than the current amplitudes needed in the feedforward schemes. However, it is of course possible to limit the feedback controller output, if the excessive output currents would be damaging. On the other hand, increased battery and electrode lifetime and less habituation of the neural response to the stimuli makes the switched interval controller and the action potential conditioned permanent state feedback controller an interesting alternative to the permanent controller. The AP conditioned permanent controller might be especially interesting for peripheral applications such as reflex modulation or achieving complete blocking of action potential propagation.

Appendix

The original Hodgkin-Huxley model (1952) of the space-clamped giant squid axon is given by the following four equations):

$$C_m \frac{dV}{dt} = \bar{G}_K n^4 (E_K - V) + \bar{G}_{\mathrm{Na}} m^3 h (E_{\mathrm{Na}} - V) + G_m (V_{\mathrm{rest}} - V) + I_{\mathrm{inj}} \quad (12)$$

$$\frac{dn}{dt} = \alpha_n(V)(1-n) - \beta_n(V) n \quad (13)$$

$$\frac{dm}{dt} = \alpha_m(V)(1-m) - \beta_m(V) m \quad (14)$$

$$\frac{dh}{dt} = \alpha_h(V)(1-h) - \beta_h(V) h. \quad (15)$$

Table 3 lists the values of the parameters used in Eq. (12). α and β are the so-called rate constants.

Table 3. Parameters for Hodgkin-Huxley equations (1999).

Maximal potassium conductance	$\bar{G}_K$	36 mS/cm^2
Sodium ionic battery	E_k	−12 mV
Maximal sodium conductance	$\bar{G}_{\mathrm{Na}}$	120 mS/cm^2
Ionic sodium battery	E_{Na}	115 mV
Leak conductance	G_m	0.3 mS/cm^2
Resting potential	V_{rest}	0 mV
Membrane capacity	C_m	1 μF/cm^2

References

Benabid A-L, Koudsi A, Benazzouz A, Fraix V, Ashraf A, Le Base JF, Chabardes S, Pollak P (2000) Subthalamic stimulation for Parkinson's disease. Archives of Medical Research 31: 282–289.

Chay TR, Lee YS (1984) Impulse responses of automaticity in the Purkinje Fiber. Biophysical Journal 45: 841–849.

Cooley J, Dodge F, Cohen H (1965) Digital computer solutions for excitable membrane models. Journal of Cellular and Comparative Physiology 66(3): 99–108.

Durand DM, Bikson M (2001) Suppression and control of epileptiform activity by electrical stimulation: A review. Proceedings of the IEEE 89: 1065–1082.

Dodge FA, Frankenhaeuser B (1959) Sodium currents in myelinated nerve. Journal of Physiology 148: 188–200.

Fitzhugh R (1962) Computation of impulse initiation and saltatory conduction in a myelinated nerve fiber. Biophysical Journal (2): 11–21.

Fukai H, Doi S, Nomura T, Sato S (2000) Hopf bifurcations in multiple-parameter space of the Hodgkin-Huxley equation I. Global organization of bistable periodic solutions. Biological Cybernetics 82: 215–222.

Fröhlich F, Jezernik, S (2003) Feedback control of Hodgkin-Huxley nerve cell dynamics. In: Proceedings of the 5th IFAC 2003 Symposium on Modelling and Control in Biomedical Systems, Melbourne, Australia, pp. 439–443.

Gluckman, BJ, Nguyen H, Weinstein SL, Schiff SJ (2001) Adaptive electric field control of epileptic seizures. The Journal of Neuroscience 21(2): 590–600.

Goldman L, Albus JS (1968) Computation of impulse conduction in myelinated fibres: Theoretical basis of the velocity-diameter relation. Biophysical Journal 8: 596–607.

Guevara MR, Shrier A (1987) Phase resetting in a model of cardiac Purkinje Fiber. Biophysical Society 52: 165–175.

Guttman R, Lewis S, Rinzel J (1980) Control of repetitive firing in squid axon membrane as a model for a neuronoscillator. Journal of Physiology 305: 377–395.

Hahn PJ, Durand DM (2001) Bistability dynamics in simulation of neural activity in high-extracellular-potassium conditions. Journal of Computational Neuroscience 11: 5–18.

Hodgkin AL, Huxley AF (1952) A quantitative description of membrane current and its application to conduction and excitation in nerve. Journal of Physiology 177: 500–544.

Hursh JB (1939) Conduction velocity and diameter of nerve. American Journal of Physiology 127: 131.

Huxley AF, Stämpfli R (1948) Evidence for saltatory conduction in peripheral myelinated nerve fibres. Journal of Physiology 108: 315–339.

Jahangiri A, Durand DM, Lin J-C (1997) Singular stimulus parameters to annihilate spontaneous activity in Hodgkin-Huxley model with elevated potassium. In: Proceedings of th 19th International Conference IEEE/EMBS, Chicago, USA, pp. 2026–2028.

Khalil HK (2002) Nonlinear Systems. 2nd edition Prentice Hall, Upper Saddle River, NJ.

Khibnik AI, Kuznetsov YA, Levitin VV, Nikolaev EV (1992) Interactive local bifurcation analyzer. http://locbif.tripod.com/.

Kiss ZHT, Mooney DM, Renaud L, Hu B (2002) Neuronal response to local electrical stimulation in rat thalamus: Physiological implications for mechanisms of deep brain stimulation. Neurosci. 113(1): 137–143.

Koch C (1999) Biophysics of Computation. Information Processing in Single Neurons. Oxford University Press, New York.

McNeal, DR (1976) Analysis of a model for excitation of myelinated nerve. IEEE Transactions on Biomedical Engineering 23(4): 329–337.

Oprisan, SA, Canavier CC (2002) The influence of limit cycle topology on the phase resetting curve. Neural Computation 14: 1027–1057.

Rattay F (1990) Electrical Nerve Stimulation. Theory, Experiments, and Applications. Springer-Verlag.

Stämpfli R (1952) Bau und Funktion isolierter markhaltiger Nervenfasern. Ergebnisse der Physiologie 47: 70.

Tass PA (2003) A model of desynchronizing deep brain stimulation with a demand-controlled coordinated reset of neural subpopulations. Biological Cybernetics 89: 81–88.

Weiss TF (1996) Electrical Properties, vol. 2 of Cellular Biophysics. MIT Press.

Winfree AT (1987) When Time Breaks Down. Princeton University Press.